J Clust Sci (2016) 27:1081–1096
DOI 10.1007/s10876-016-0969-z

REVIEW

BN Nanotube Serving as a Gas Chemical Sensor for N_2O by Parallel Electric Field

Mohammad T. Baei[1] · A. S. Ghasemi[2] · E. Tazikeh Lemeski[3] · Alireza Soltani[4,5] · Niloofar Gholami[5]

Received: 3 August 2015 / Published online: 9 March 2016

Abstract Density functional theory calculations were performed to understand the electronic properties of C_{24}, $B_{12}N_{12}$, $B_{12}P_{12}$, and (6, 0) BNNT interacted with N_2O molecule in the presence and absence of an external electric field using the B3LYP method and 6-31G** basis set. The adsorption of N_2O from O-side on the surface of (6, 0) BNNT has high sensitivity in comparison with $B_{12}N_{12}$ nano-cage. The adsorption energy of N_2O (O-side) on the sidewalls of $B_{12}N_{12}$ and BNNT in the presence of an electric field are -21.01 and -15.48 kJ mol^{-1}, respectively. Our results suggest that in the presence of an electric field, the $B_{12}N_{12}$ nano-cage is the more energetically notable upon the N_2O adsorption than (6, 0) BNNT, C_{24}, and $B_{12}P_{12}$. Whereas, our results indicate that the electronic property of BNNT is more sensitive to N_2O molecule at the presence of an electric field than $B_{12}N_{12}$ nano-cage. It is anticipated that BNNT could be a favorable gas sensor for the detection of N_2O molecule.

Keywords BN nanostructures · N_2O · Electric field · Density functional theory

✉ Alireza Soltani
alireza.soltani46@yahoo.com

[1] Department of Chemistry, Azadshahr Branch, Islamic Azad University, Azadshahr, Golestan, Iran

[2] Department Chemistry, Payame Noor University, P.O. Box, 19395-3697, Tehran, Iran

[3] Department of Chemistry, Gorgan Branch, Islamic Azad University, Gorgan, Iran

[4] Joints, Bones and Connective Tissue Research Center, Golestan University of Medical Science, Gorgan, Iran

[5] Young Researchers and Elite Club, Gorgan Branch, Islamic Azad University, Gorgan, Iran

Introduction

Since the discovery of C_{60} [1], carbon nano-cage structures such as fullerene-like nano-cages, nanotubes, nanocapsules, nanopolyhedra, cones, cubes, and onions were studied [2–4]. Boron nitride (BN) nanostructures with energy gap of $\sim$6 eV and non-magnetism are also expected to show various electronic, optical and magnetic properties such as Coulomb blockade, photoluminescence, and super magnetism [5]. Several studies have been reported on BN nanomaterials such as BN nanotubes, BN nanocapsules, BN nanoparticles, and BN clusters, which are expected to be useful as electronic devices, high heat-resistance semiconductors, insulator lubricants and gas storage materials [6–12]. Some BN nanocages have theoretically been predicted [12], and BN clusters with sizes of 1 nm were observed only by high-resolution electron microscopy (HREM), which is a powerful method for direct observation of the atomic structure of clusters. BN metallofullerenes, which showed the possible existence of metal atoms inside the $B_{36}N_{36}$ clusters, were also reported from HREM. For these BN clusters, $B_{12}N_{12}$ cluster was theoretically predicted to be the smallest cage cluster satisfying the isolated tetragonal rule, BN cluster solids were also predicted. Although the $B_{12}N_{12}$ clusters were reported by HREM, mass spectrum analysis has been mandatory for determining the existence of $B_{12}N_{12}$ nano-cages, and a few such reports that have been presented [2, 13–20]. The purpose of the present work is to study of N_2O adsorption on the electronic properties of C_{24}, $B_{12}N_{12}$, $B_{12}P_{12}$ nano-cages and (6, 0) BNNT using DFT calculations. To understand the atomic structure models and structural stabilities of the clusters, total energy calculations were carried out by B3LYP method. Farmanzadeh and Ghazanfary [21] have investigated the effect of field emission properties on the *zigzag* (4, 0) BNNT. Attaccalite et al. computed the optical absorption spectra of BN nanotubes in the presence of a perpendicular electric field and demonstrated that the optical spectra of BNNTs are quite robust to the application of an external field [22]. Yuan and Zhao studied transport properties and induced voltage in the structure of water-filled SWBNNTs using density functional theory (DFT)/molecular dynamic (MD) simulations [23]. Based on the methods of density functional theory and molecular dynamic calculations, Yuan and Zhao investigated the voltage induced by the structure of water-filled single-walled carbon nanotube [24]. In the previous report, we have investigated the adsorption of N_2O molecule on the surfaces of CNTs and BNNTs [25, 26]. In recent years, several studies have studied the computational calculation of the field effects on the electronic and structural properties of nanotubes [22, 27, 28]. Machado et al. have investigated on zigzag and armchair single-walled aluminum nitride nanotubes in various diameters under the influence of just perpendicular external electric fields in 0.3 and 0.5 V/Å. They have shown that tubes with larger diameters are more stable and the applied perpendicular external electric fields do not have significant influence on the stability of these structures [29]. We have shown that the Al-doped CNTs have high sensitivity to the presence of N_2O molecule in comparison with the perfect CNTs [25]. In the present study, we are going to investigate the adsorption properties of N_2O molecule on the surfaces of BN nanotube and $B_{12}N_{12}$ nano-

cluster in the presence of the parallel electric fields using density functional theory (DFT). The relaxed geometries, chemical potential (μ), global softness (S), global hardness (η), and electrophilicity index (ω) [8, 9] were studied for the most stable state and compared with the perfect applied clusters and nanotubes. We hope that our calculations provide better conditions for Nitrous Oxide (N_2O) sensor design.

Computational Details

Geometry optimizations, molecular electrostatic potential (MEP), frontier molecular orbital (FMO), natural bond orbital (NBO), and density of states (DOS) analyses were performed on the C_{24}, $B_{12}N_{12}$, $B_{12}P_{12}$, and (6, 0) BNNT. All the geometry optimizations and energy calculations are done by using GAMESS software [30] at the level of density functional theory (DFT) using B3LYP method and 6-31G** basis set [31–35]. The basis set superposition error (BSSE) for the adsorption energy was corrected implementing the counterpoise method [36]. The adsorption energies (E_{ad}) were computed using the formula:

$$E_{ad} = E_{nano-cage-N2O} - \left(E_{nano-cage} + E_{N2O}\right) + E_{BSSE} \quad (1)$$

$$E_{ad} = E_{nanotube-N2O} - \left(E_{nanotube} + E_{N2O}\right) + E_{BSSE} \quad (2)$$

where $E_{nano\text{-}cage\text{-}N2O}$ and $E_{nanotube\text{-}N2O}$ are the total energies of the C_{24}, $B_{12}N_{12}$, $B_{12}P_{12}$, and BNNT interacting with the N_2O molecule. $E_{nano\text{-}cage}$ and $E_{nanotube}$ are the total energies of the pure C_{24}, $B_{12}N_{12}$, $B_{12}P_{12}$, and BNNT, respectively, and E_{N2O} is the total energy of an isolated N_2O. The electrophilicity index (ω) concept was stated for the first time in 1999 by Parr et al. [37]. Chemical potential (μ) is defined according to the following equation:

$$\mu = -\chi = -(I + A)/2 \quad (3)$$

electronegativity (χ) is defined as the negative of chemical potential, as follows: $\chi = -\mu$. Furthermore, chemical hardness (η) can be approximated using the Koopmans' theorem [38] I ($-E_{HOMO}$) is the ionization potential and A ($-E_{LUMO}$) the electron affinity of the molecule. Where E_{HOMO} is the energy of the Fermi level and E_{LUMO} is the first given value of the conduction band. $\eta = (I - A)/2$. Softness (S) and electrophilicity index are determined as the following equations, respectively.

$$S = 1/2\eta \quad (4)$$

$$\omega = \left(\mu^2/2\eta\right) \quad (5)$$

Results and Discussion

N_2O Adsorption in the Perfect $B_{12}N_{12}$

First of all, we are going to explore the binding energy of nitrous oxide (N_2O) on the surface of $B_{12}N_{12}$. We have fully relaxed the geometry at the B3LYP/6-31G** level of the theory. The O and N atoms in the N_2O molecule approached to the $B_{12}N_{12}$ surfaces are shown in Fig. 1. After the adsorption of N_2O molecule on $B_{12}N_{12}$ nano-cage, the bond lengths of these adsorption formations (a–d) have undergone slight changes in comparison with the pristine $B_{12}N_{12}$ nano-cage. For configurations (a–d), the adsorption energies of N_2O molecules from oxygen head on the sidewall of $B_{12}N_{12}$ are about −4.51, −7.10, −7.83, and −8.37 kJ mol^{-1}, the interaction

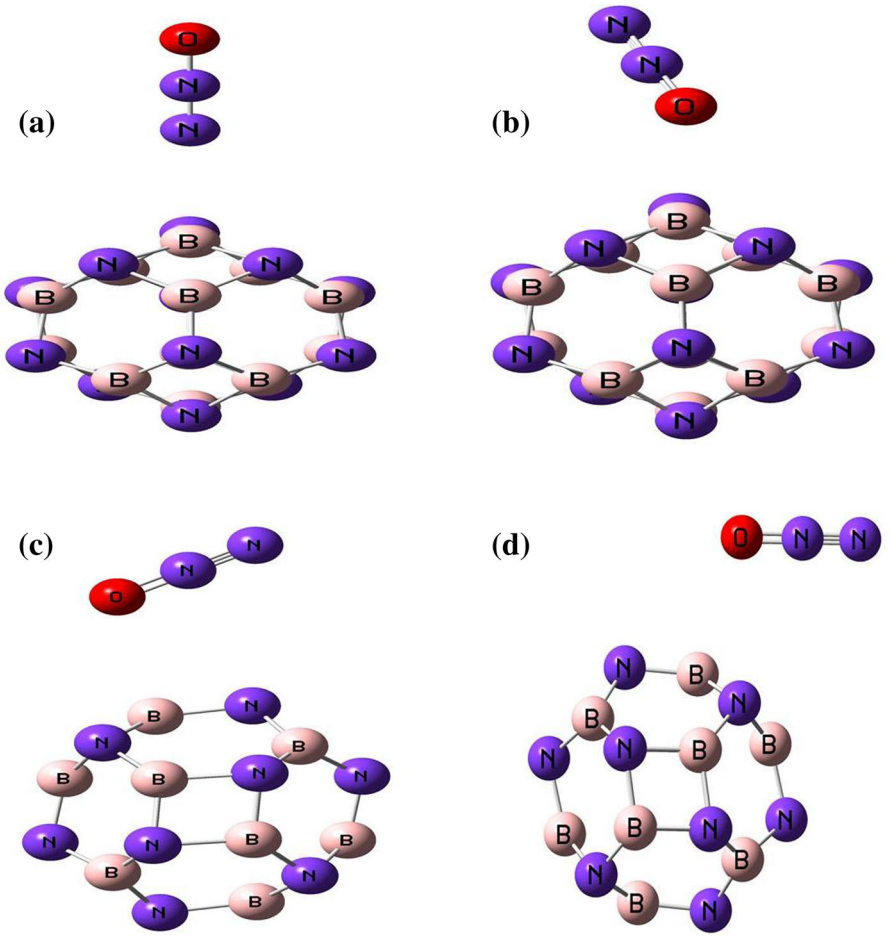

Fig. 1 The optimized configurations of N_2O adsorption upon the $B_{12}N_{12}$ by the nitrogen and oxygen attacking (**a–d**)

distances between the N_2O and the $B_{12}N_{12}$ are 2.99, 2.72, 2.70, and 2.68 Å, respectively (see Fig. 1).

The comparable values after BSSE correction for these configurations are about −1.94, −2.32, and −2.60 kJ mol^{-1}, respectively. After BSSE correction, we have found that the adsorption energy for N_2O from nitrogen head with the interaction distance of 3.01 Å declines from −4.50 to −0.6 kJ mol^{-1} at the B3LYP/6-31G** level of computation. The small binding energies and large distances demonstrate weak physical adsorption on the outer surface of nano-cage due to weak Van der Waals interaction [39]. In the most stable state of N_2O (O-side) a slight charge about 0.04e is transferred from the cluster to the N_2O molecule. The current computations

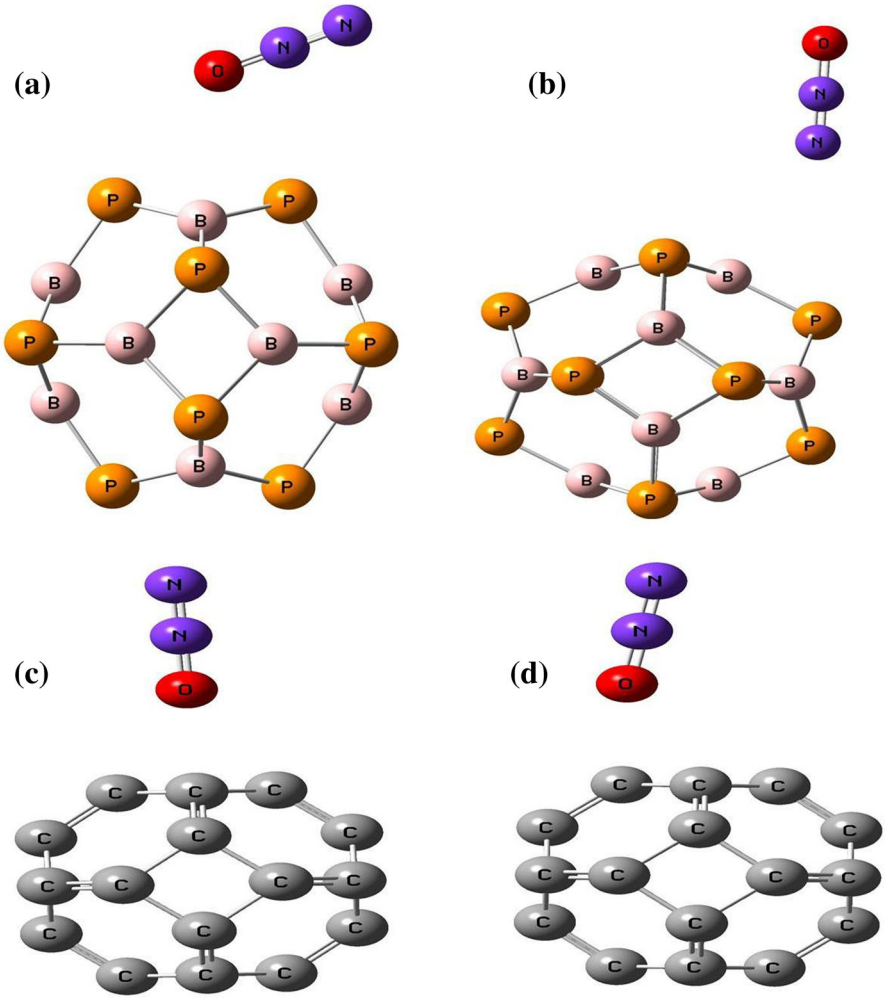

Fig. 2 The optimized configurations of N_2O adsorption upon the C_{24} and $B_{12}P_{12}$by the nitrogen and oxygen attacking (**a–d**)

indicate that the bond lengths of $B_{12}N_{12}$ before and after adsorption of N_2O changed from 1.439 to 1.444, 1.440, and 1.445 Å in the configurations (b), (c), and (d).The results demonstrate that the binding energy of nitrous oxide is higher than that of CNTs and BNNTs [25, 26]. Second, we are investigated the interaction of N_2O molecule on the walls of $B_{12}P_{12}$ and C_{24} nano-cages (see Fig. 2).

The adsorption energy values of N_2O molecule (O-side and N-side) on the exterior sidewall of $B_{12}P_{12}$ were in the ranges of -1.68 and -0.25 kJ mol^{-1} and the

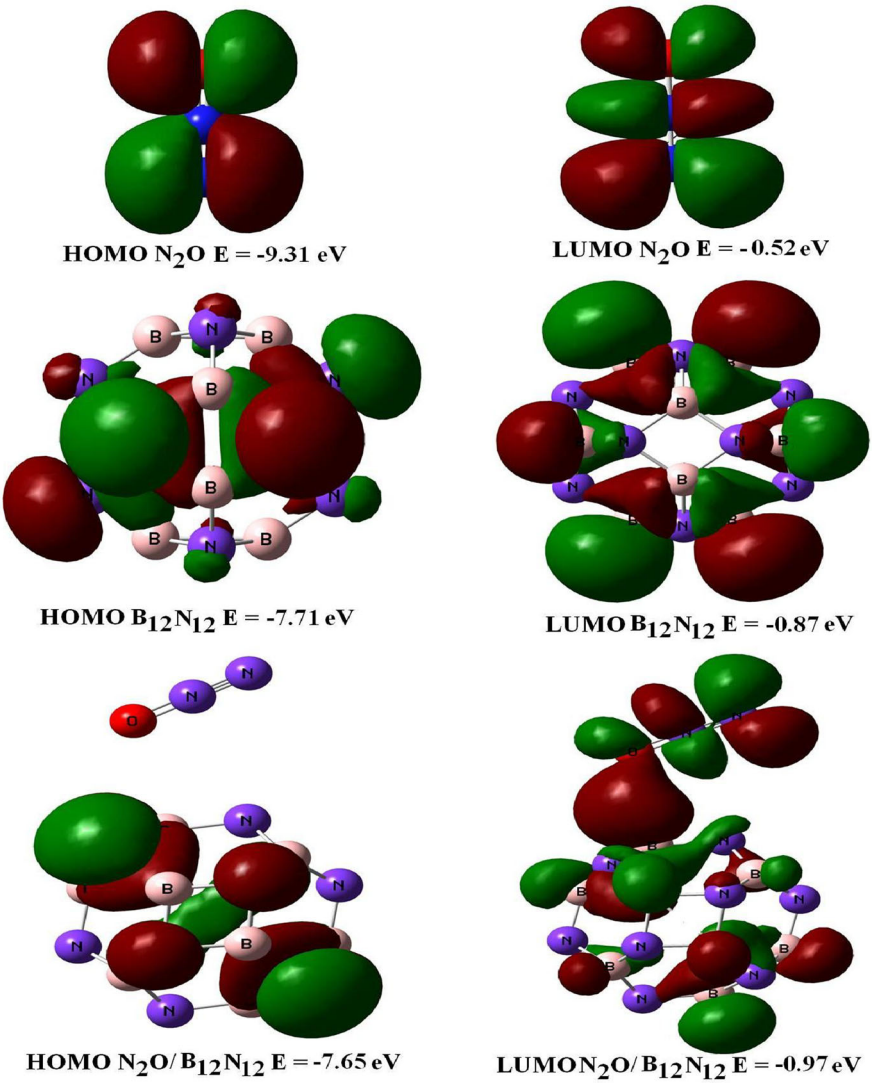

Fig. 3 Isosurface of the HOMO and LUMO orbitals of the N_2O molecule, $B_{12}N_{12}$, and the most stable complex of $N_2O/B_{12}N_{12}$

distances of O and N atoms of N_2O upon a B atom of $B_{12}P_{12}$ are about 3.26 and 3.53 Å, respectively. NBO charge analysis indicates that the charge transfer from $B_{12}P_{12}$to N_2O is about 0.01e. On the other hand, we have found that the values of N_2O adsorption (O-side and N-side) on the C_{24} surface are −1.04 and −0.10 kJ mol^{-1}, the C–O and C–N distances are 3.37 and 3.73 Å, respectively, the binding energies of N_2O on the surfaces of $B_{12}P_{12}$ and C_{24} revealed the physisorption nature of the adsorption processes (Fig. 2). NBO computation shows that the net charge transfer from C_{24} to N_2O is about 0.001e. In contrast, N_2O adsorptions on the clusters of the most stable states were determined as follows: $B_{12}N_{12} > B_{12}P_{12} > C_{24}$.

In order to comprehend the adsorption energy of N_2O molecule for the most stable configuration on B atom of $B_{12}N_{12}$, we are considered the highest occupied molecular orbital (HOMO) of $B_{12}N_{12}$ being localized upon the N atoms with the energy level of −7.71 eV, while the lowest unoccupied molecular orbital (LUMO) is localized on the B–N bonds of nano-cage in energy level about −0.87 eV. The position of HOMO for the $N_2O/B_{12}N_{12}$complex is located toward the N atoms of $B_{12}N_{12}$ and the energy level in there is about −7.65 eV. The LUMO for this complex is distributed into the O=N=N bonds and the B atom of $B_{12}N_{12}$ is located upon the B–N bonds of nanocluster and the energy level of LUMO is −0.97 eV (see Fig. 3; Table 1).

The calculations indicate that the energies of HOMO and LUMO of N_2O molecule are about −9.31 and −0.52 eV, respectively. The smallest change of energy gap (E_g) belongs to the configuration (**c**) indicating that the E_g of this complex is reduced from 6.84 to 6.68 eV, which is an insignificant alteration. Therefore, it can be deduced that the nitrous oxide may not affect the electrical

Table 1 E_{LUMO} and E_{HOMO}, Dipole moment (μ_D/Debye), energy gap (E_g), change of bond gap (ΔE_g), energy of Fermi level (E_F) and quantum molecular descriptors values of N_2O adsorption on $B_{12}N_{12}$ at the B3LYP method in the absence of an external electric field

Property	N_2O	$B_{12}N_{12}$	$N_2O/B_{12}N_{12}$(O-side)	$N_2O/B_{12}N_{12}$(N-side)
E_{HOMO}/eV	−9.31	−7.71	−7.65	−7.53
E_{LUMO}/eV	−0.52	−0.87	−0.97	−0.84
E_g/eV	8.79	6.84	6.68	6.79
ΔE_g (%)	–	–	−2.34	−0.73
μ_D/Debye	0.01	0.00	0.52	0.53
E_{ad}/kJ mol^{-1}	–	–	−8.37	−4.50
E_F/eV	−4.91	−4.29	−4.31	−4.23
I/eV	9.31	7.71	7.65	7.53
A/eV	0.52	0.87	0.97	0.84
η/eV	4.39	3.42	3.34	3.34
μ/eV	−4.91	−4.29	−4.31	−4.18
S/eV^{-1}	0.11	0.15	0.15	0.15
ω/eV	2.75	2.69	2.78	2.62

conductivity of $B_{12}N_{12}$. Calculated the electronic properties of $B_{12}N_{12}$ interacted with N_2O in comparison with perfect nano-cage. The total DOS of N_2O, $B_{12}N_{12}$, and $N_2O/B_{12}N_{12}$ complexes are presented in Fig. 4.The adsorption capabilities for all configurations indicate that the DOS near the Femi level (E_F) is not affected after the N_2O adsorption. On the other word, the energy gap of nano-cage after the adsorption of N_2O has no significant change. Therefore, we believe that the $B_{12}N_{12}$ may not be a suitable sensitive device for toxic N_2O detection. Thus, we limited static the external electric field effect to the interaction of N_2O at $B_{12}N_{12}$ nano-cage.

Electrical Field Emission Properties on the $B_{12}N_{12}$

We considered the behavior of N_2O adsorption upon the $B_{12}N_{12}$ by the external parallel electric fields (E_X) at the B3LYP method. The current calculations show that binding energy for the most stable configuration of N_2O adsorbed from N-side on the $B_{12}N_{12}$ is rather weak compared with its O-side, while growths in the electric field intensities for N_2O adsorbed on the $B_{12}N_{12}$ have been largely altered in comparison with the binding energy of N_2O on the nano-cages in the absence of an external electric field. The interaction of N_2O molecule presented in the parallel electric field (E_X) upon the $B_{12}N_{12}$ was studied, revealing that E_X is the static electric field effect on the positive X direction. The numerical values of the parallel

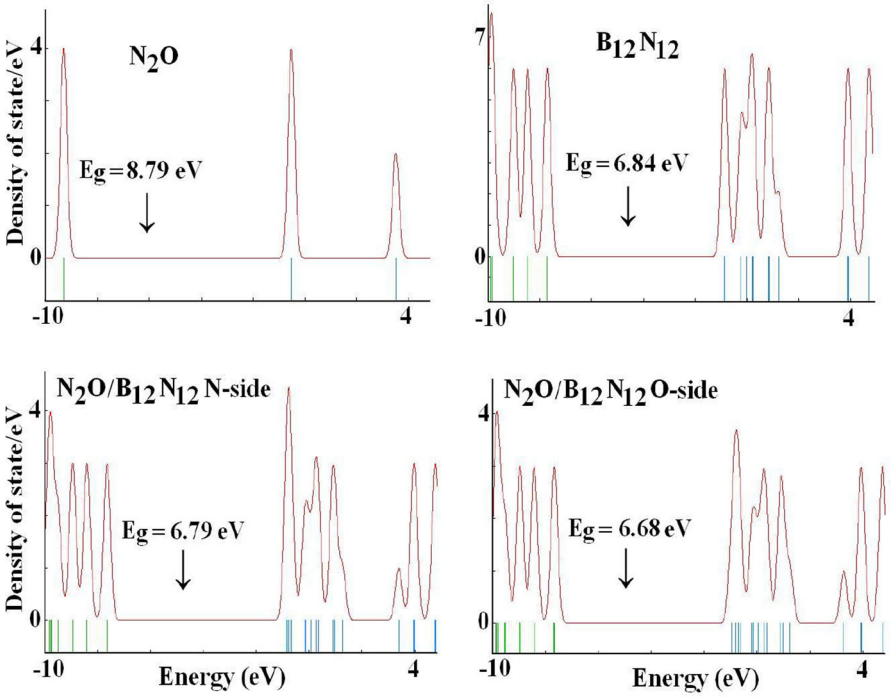

Fig. 4 Calculated DOS plots of the pure $B_{12}N_{12}$, N_2O, and $N_2O/B_{12}N_{12}$ complex

field strengths applied on the $B_{12}N_{12}$ are 0.005, 0.01, 0.02 a.u. (1 a.u. = 514.224 V/nm) [21]. We considered the electronic properties of the $B_{12}N_{12}$ including adsorption energies, electric dipole moments, molecular orbital energy, DOS, and electronic spatial extent upon the ranges of 0–0.02 a.u. Under an electric field, When N_2O molecule (O-side) adsorbed on the $B_{12}N_{12}$ surface, the adsorption energy is obviously increased for the most stable configuration (O-side) from -8.37 kJ mol^{-1} at zero field strength to -9.65, -11.00, and -21.01 kJ mol^{-1} at the field strength of 0.005, 0.01, and 0.02 a.u., respectively. The results indicate that the interaction energies of N_2O adsorbed on the $B_{12}N_{12}$ surface monotonically raise

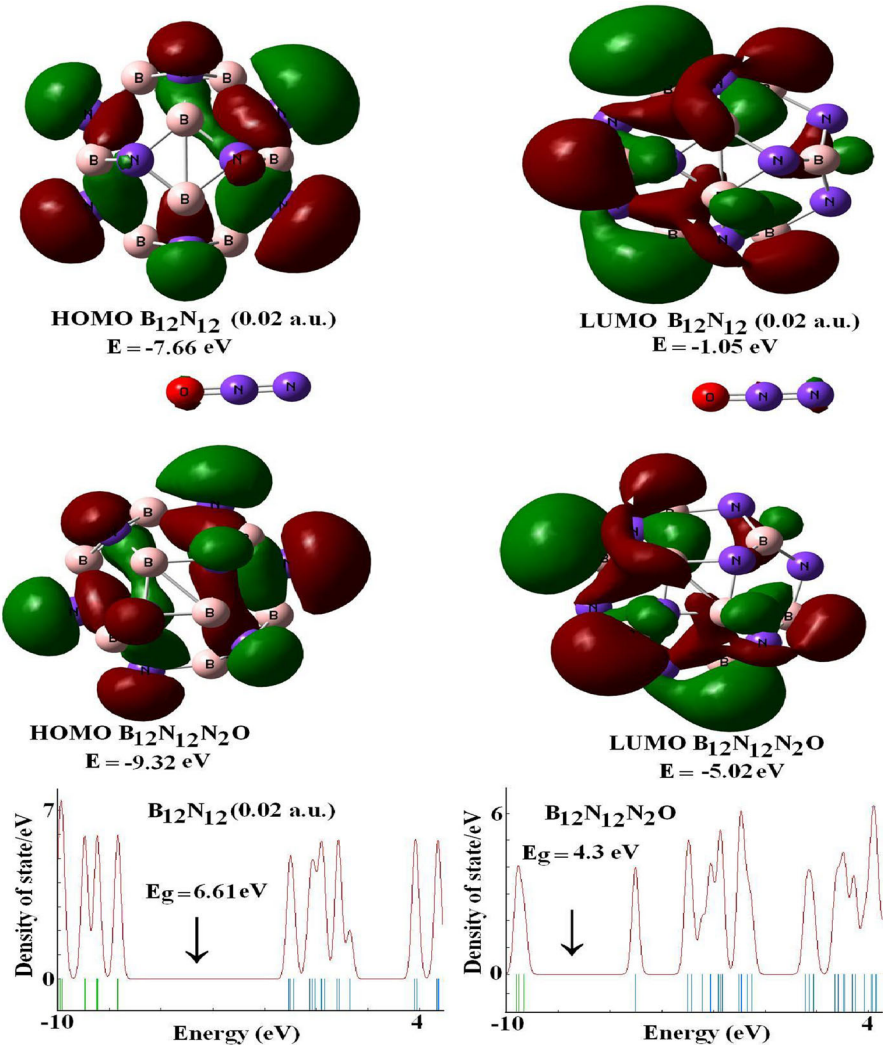

Fig. 5 Profiles of the HOMO and LUMO orbitals of the pure $B_{12}N_{12}$ and $N_2O/B_{12}N_{12}$ complex in the presence of an electric field

with rising numbers of the parallel electric field effects. The bond distances of $B_{12}N_{12}$ under the electric field effects before and after the adsorption change from 1.441 to 1.455, 1.455, and 1.469 Å at the field strength of 0.005, 0.01, 0.02 a.u., respectively. For N_2O adsorbed on the surface of $B_{12}N_{12}$, the bond lengths of N=O and N=N changed about (1.869 and 1.136 Å), (1.870 and 1.136 Å), and (1.178 and 1.140 Å) in the field strength of 0.005, 0.01, 0.02 a.u., respectively, and the bond angles of O=N=N are altered in free N_2O and $N_2O/B_{12}N_{12}$ complex from 180.0° to 179.53°, 179.54°, and 178.44° at the field strength of 0.005, 0.01, 0.02 a.u., respectively. Li and Wang have reported that the binding energy of gas molecules in the presence of a strong electric field is very remarkable in comparison with the absence of the electric field [39]. The dipole moment values obviously increased under an external electric field from 2.22, 4.45, and 8.95 Debye in the pristine $B_{12}N_{12}$ to 3.21, 5.05, and 10.38 Debye in the N_2O–$B_{12}N_{12}$ complexes at the field strength of 0.005, 0.01, 0.02 a.u., respectively. The results indicate that the dipole moment values for these complexes in the presence of electric field increases in comparison with zero field strength in the perfect $B_{12}N_{12}$ nano-cluster [40, 41]. We compared the frontier molecular orbital (FMO) of N_2O and $B_{12}N_{12}$ system. Under a strong electric field (0.02 a.u.), the HOMO of $B_{12}N_{12}$ is more located on the nitrogen atoms of cluster with energy about −7.66 eV, while the LUMO of cluster is localized toward the B–N bonds with energy about −1.05 eV. The position of HOMO and LUMO for $N_2O/B_{12}N_{12}$ complex is also localized on the N atoms and B–N bonds of $B_{12}N_{12}$ and is slightly localized on O and N atoms of N_2O molecule with the energies at about −9.32 and −5.02 eV, respectively (Fig. 5). The evolution of the LUMO of the complex in the presence of an electric field is asymmetric. As

Table 2 E_{LUMO} and E_{HOMO}, Dipole moment/μ_D (Debye), energy gap (E_g), change of bond gap (ΔE_g), energy of Fermi level (E_F) and quantum molecular descriptors values of N_2O adsorption on BNNT and $B_{12}N_{12}$ at the B3LYP method in the presence of an external electric field

Property	(6,0) BNNT	$B_{12}N_{12}$	N_2O/BNNT (O-side)	$N_2O/B_{12}N_{12}$(O-side)
E_{HOMO}/eV	−6.71	−7.66	−7.72	−9.32
E_{LUMO}/eV	−1.59	−1.05	−5.60	−5.02
E_g/eV	5.12	6.61	2.12	4.3
ΔE_g (%)	–	–	−58.6	−34.95
μ_D/Debye	33.60	8.95	34.68	10.38
E_{ad}/kJ mol^{-1}	–	–	−15.48	−21.01
E_F/eV	−4.15	−4.35	−6.66	−7.17
I/eV	6.71	7.66	7.72	9.32
A/eV	1.59	1.05	5.60	5.02
η/eV	2.56	3.30	1.06	2.15
μ/eV	−4.15	−4.35	−6.66	−7.17
S/eV^{-1}	0.19	0.15	0.47	0.23
ω/*eV*	3.36	2.87	20.92	11.95

can be seen in Fig. 5, the LUMO energy after N_2O adsorption on the surface of $B_{12}N_{12}$ is significantly changed in comparison with the HOMO energy.

Moreover, the difference energy gap (E_g) between HOMO and LUMO is considered to be a notable factor in chemical reactivity levels of nano-cages. A small energy gap leads to the low chemical stability, since it is energetically noticeable to add electrons to a high-lying LUMO or to extract electrons from a low-lying HOMO. In Fig. 5, DOS indicates that the electronic properties of the $B_{12}N_{12}$ under an electric field have significant changes toward the adsorption of N_2O molecule. Under an electric field (0.02 a.u.), the energy gap of $B_{12}N_{12}$ has a noticeable change from 6.61 to 4.3 eV with the addition of N_2O molecule (see Table 2). The results of the DOS demonstrate remarkable changes in the energy gap

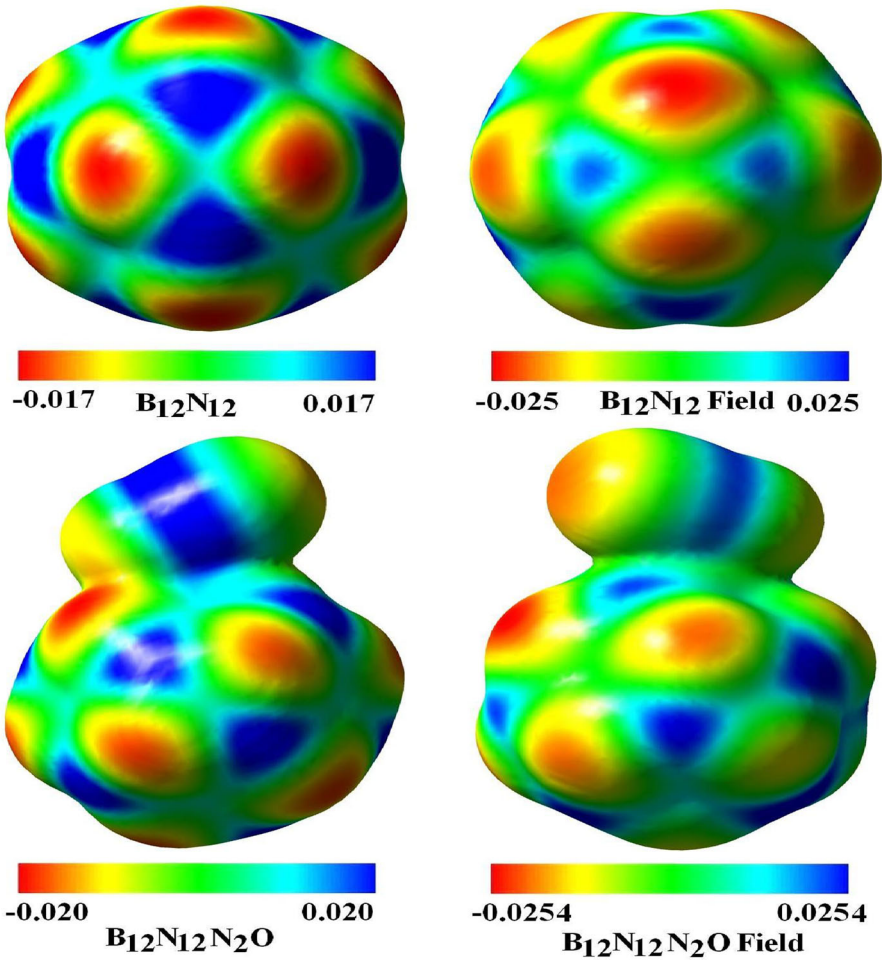

Fig. 6 MEP plots of the pure N_2O, $B_{12}N_{12}$, and $N_2O/B_{12}N_{12}$ complex in the presence and absence of an electric field

due to adsorption of N_2O molecule, resulting in diminution of energy gap that leads to increase of electrical conductivity. This result demonstrates that the N_2O adsorption upon $B_{12}N_{12}$ under an electric field has significantly affected the electronic structure of $B_{12}N_{12}$ nano-cage. As a result, the pure $B_{12}N_{12}$ can be applied as a N_2O sensor and increasing the parallel electric field effect that is an applicable method for N_2O adsorption on $B_{12}N_{12}$ nano-cage. MEP plots of single $B_{12}N_{12}$ nano-cage interacted with the N_2O molecule in the presence and absence of an external electric field are shown in Fig. 6. In the pure $B_{12}N_{12}$ nano-cage with an electric field, the B atoms are positively charged (blue colors) and the N atoms of the structure are negatively charged (red colors), whereas in the presence of an

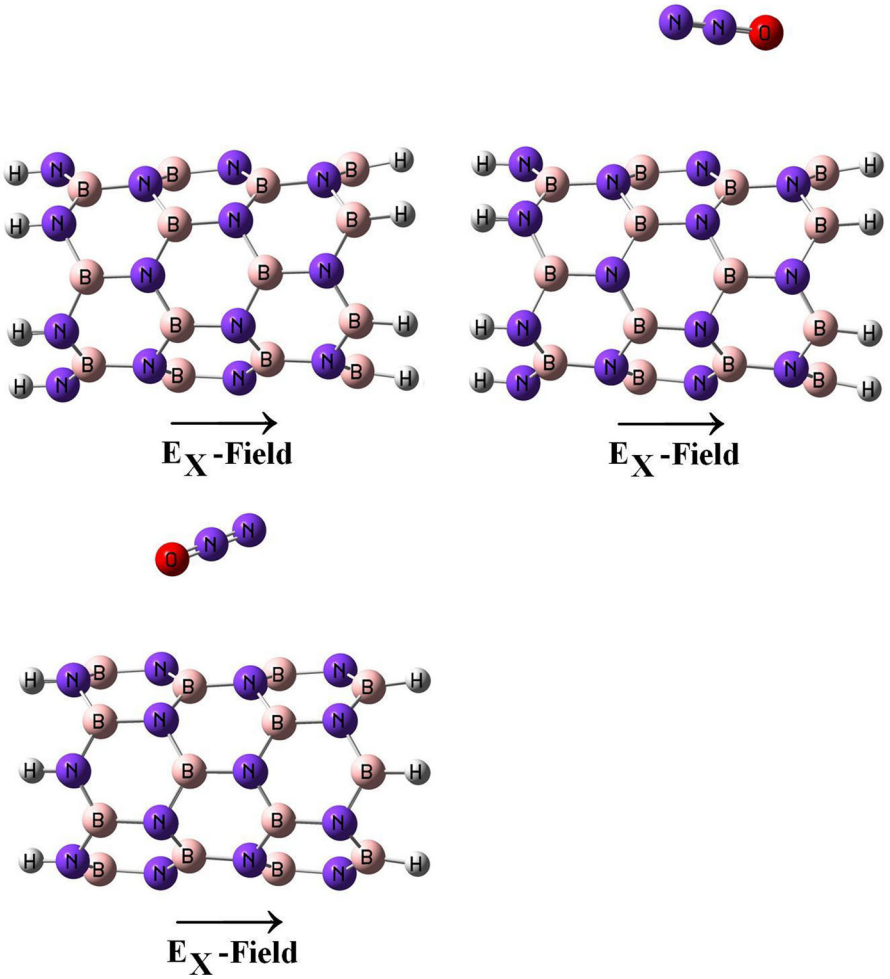

Fig. 7 The optimized structures of the perfect BNNT and N_2O/BNNT system in the presence of an electric field

external electric field, the electrostatic potential going from positive to neutral (green colors).

As shown in Fig. 9, the O and N atoms of the N_2O adsorbed on $B_{12}N_{12}$ nano-cage have negative (red or yellow) and positive (blue) charges, respectively.

Electrical Field Emission Properties on the (6, 0) zigzag BNNT

We explored the influence of external electric field upon the electronic structure of the (6, 0) BNNT interacted with N_2O molecule (Fig. 7). At zero electric field ($E_X = 0$), the B–N bond length of (6, 0) BNNT changes from 1.449 to 1.482 Å under the parallel electric field ($E_X = 0.02$ a.u.), while the N–B–N bond angle does not obviously changed from 119.9 in the absence of an electric field to 118.7°,with a

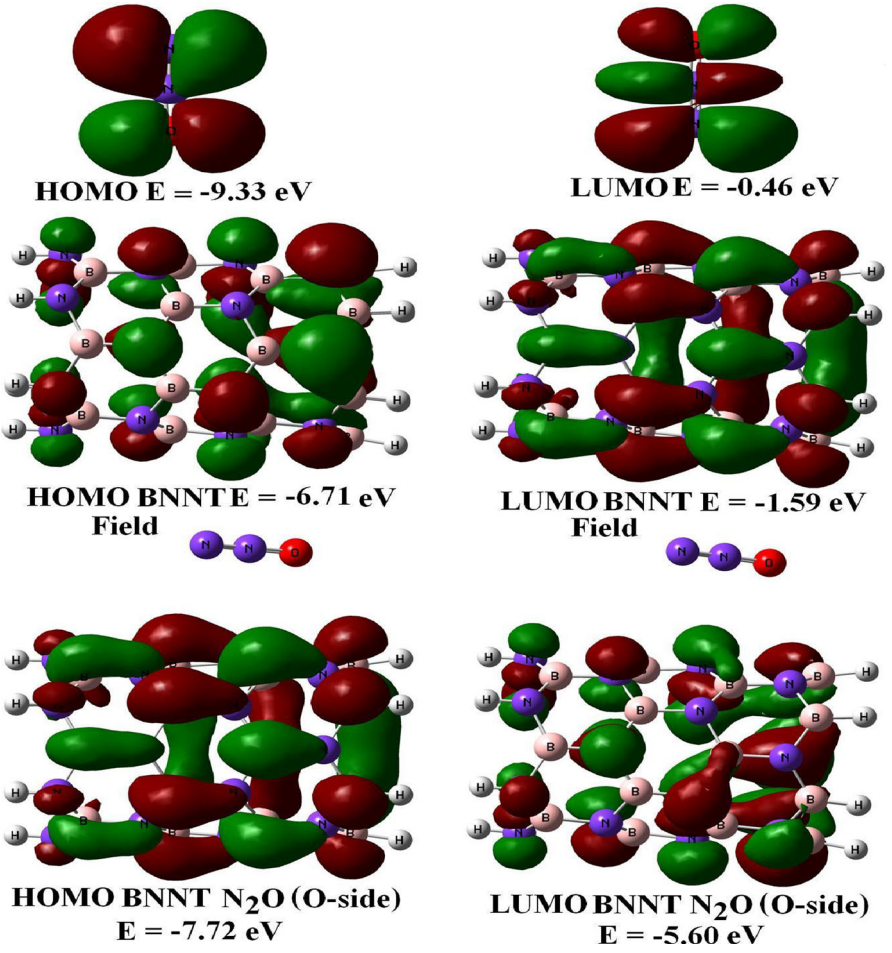

Fig. 8 Profiles of the HOMO and LUMO orbitals of the pure N_2O, $B_{12}N_{12}$, and $N_2O/B_{12}N_{12}$ complex in the presence of an electric field

parallel electric field ($E_X = 0.02$ a.u.). The bond length of B–N after the N_2O adsorption on the surface of BNNT is 1.483 Å. When a parallel electric field is applied along for N_2O/(6, 0) BNNT complex, the structural changes are rather small under strong electric field (0.02 a.u.). After the N_2O adsorption on the BNNT, the $N \equiv N$ and N=O bond lengths of N_2O molecule after the N_2O adsorption are 1.129 and 1.201 Å, respectively (Fig. 7).

In Fig. 7, we can find the adsorption energy of N_2O molecule for the most stable configurations (N-side and O-side) upon the wall of (6, 0) BNNT being about -13.63 and -15.48 kJ mol^{-1} with the distances of 3.5 and 3.2 Å, respectively. Under an electric field, the adsorption energy for N_2O in O-side is more than that in N-side in comparison with CNT and BNNT without presence of an electric field [25, 26]. The value of dipole moment (D_M) for (6, 0) BNNT in the absence and presence of electric field revealed remarkable change from 7.96 to 33.60 Debye (see

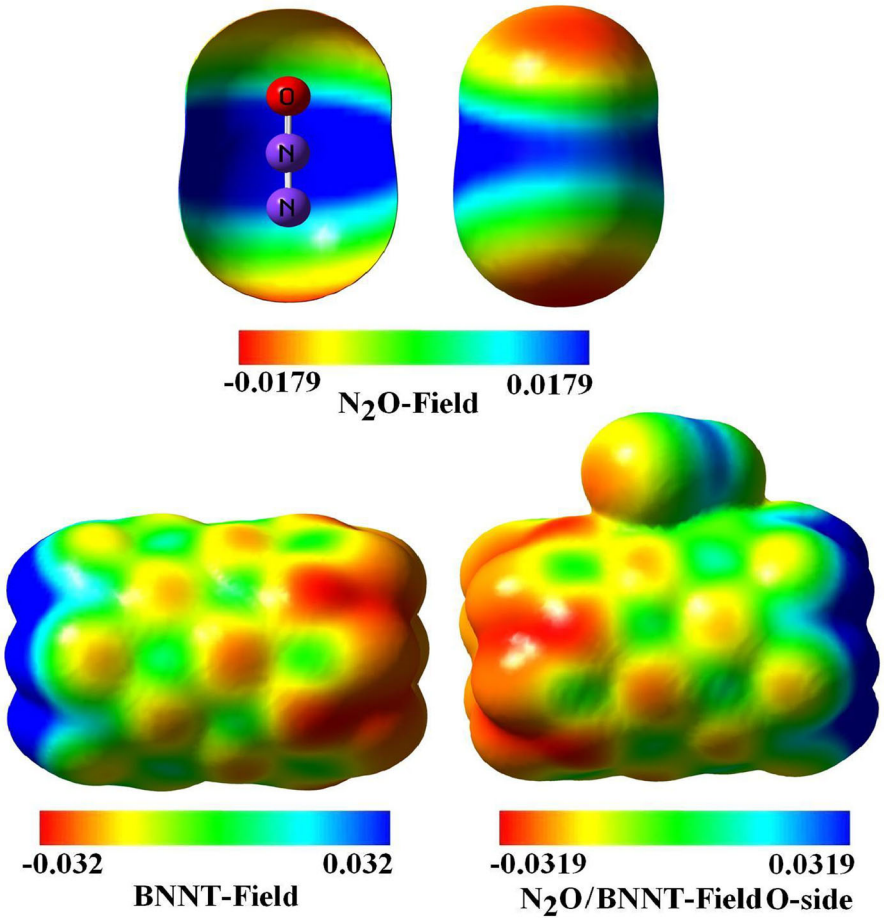

Fig. 9 Profiles of the MEP PLOTS of the pure N_2O, BNNT, and N_2O/BNNT complex in the presence of an electric field

Table 2). The result shows that in comparison with the perfect BNNT, the D_M of N_2O/BNNT complex under an electric field (0.02 a.u.) does not reveal notable change (about 34.64 Debye). We considered the influence of N_2O adsorption in the presence of an electric field upon the electronic structure of BNNT. We observe that the energy gap of (6, 0) BNNT in the absence of an external electric field increases from 4.89 to 5.12 eV in the presence of an external electric field [26]. This result indicates that the presence of an electric field increases its electrical resistivity. On the other hand, under the electric field, the energy gap of N_2O/BNNT complex for the most stable configuration has imposed significant change ($\Delta E_g = -58.6$ %) onto the adsorption process (Table 2). The presence of N_2O molecule on the wall of BNNT declines the energy gap from 5.12 to 2.12 eV, thus dramatically increases their electrical conductance [42]. We observed that the interaction between BNNT and N_2O molecule leads to alteration of the electronic structure of nanotube. Besides, FMO analysis upon N_2O/BNNT complex demonstrates that its HOMO is localized upon the B–N bonds of the tube (see Fig. 8), while the LUMO is slightly more located onto the N atoms of the nanotube.

The NBO analysis indicates that the interaction leads to charge transfer of 0.012e from the BNNT to the N_2O molecule. The molecular electrostatic potential (MEP) plots for N_2O of O head toward the BNNT surface demonstrate that the O atom of N_2O is much stronger than that of the N atom of molecule in the adsorption process (see Fig. 9). In order to indicate the sensitivity of the BNNT upon the N_2O molecule, we explored the DOS of this complex and then we compared it to the pure BNNT. The DOS of the N_2O adsorbed on the surface of tube represented that the electronic structure of BNNT in the presence of strong electric field is very sensitive upon the N_2O adsorption [43]. Therefore, the DOS of the N_2O/BNNT complex indicates changes because of N_2O adsorption in the gap regions of the TDOS plots (see Table 2).

Conclusion

By using DFT calculations, we have studied the adsorption properties of N_2O molecule onto the C_{24}, $B_{12}N_{12}$, $B_{12}P_{12}$, and (6, 0) BNNT at the B3LYP/6-31G** level of theory. Our calculations indicate that the adsorption of N_2O molecule on the surface of these nano-cages in the absence of an electric field are unable (weak physical adsorption) to render dramatic changes in the density of states near the Fermi level. Our results show a high sensitivity for (6, 0) BNNT in the presence of an electric field compared with $B_{12}N_{12}$ nano-cage for the detection of N_2O molecule.

Acknowledgments We should thank the clinical Research Development Unit (CRDU), Sayad Shirazi Hospital, Golestan University of Medical Sciences, Gorgan, Iran.

References

1. H. W. Kroto, J. R. Heath, S. C. O'Brien, R. F. Curl, and R. E. Smalley (1985). *Nature* **318**, 162.

2. R. T. Paine and C. K. Narula (1990). *Chem. Rev.* **90**, 73.
3. J. Beheshtian, A. A. Peyghan, Z. Bagheri, Kamfiroozi, Struct. Chem. doi: 10.1007/s11224-012-9970-9.
4. N. Krainara, F. Illas, and J. Limtrakul (2012). *Chem. Phys. Lett.* **537**, 88.
5. A. Rubio, J. Corkill, and M. Cohen (1994). *Phys. Rev. B* **49**, 5081.
6. T. Oku, T. Hirano, M. Kuno, T. Kusunose, K. Niihare, and K. Suganuma (2000). *Mater. Sci. Eng. B* **74**, 206.
7. T. Oku, M. Kuno, H. Kitahara, and I. Nartia (2001). *Int. J. Inorg. Mater.* **3**, 597.
8. A. Soltani, N. Ahmadian, A. Amirazami, A. Masoodi, E. Tazikeh Lemeski, and A. Varasteh Moradi (2012). *Appl. Surf. Sci.* **261**, 262.
9. A. Soltani, S. Ghafouri Raz, V. Joveini Rezaei, A. Dehno Khalaji, and M. Savar (2012). *Appl. Surf. Sci.* **263**, 619.
10. A. Soltani, M. T. Ramezani, H. Mighani, A. A. Pahlevani, and R. Mashkoor (2012). *Appl. Surf. Sci.* **259**, 637.
11. A. Soltani, N. Ahmadian, Y. Kanani, A. Dehno Khalaji, and H. Mighani (2012). *Appl. Surf. Sci.* **258**, 9536.
12. J. Beheshtian, Z. Bagheri, M. Kamfiroozi, and A. Peyghan (2011). *Microelectron J.* **42**, 1400.
13. A. V. Pokropivny (2006). *Diam. Relat. Mater.* **15**, 1492.
14. T. Oku, A. Nishiwaki, and I. Narita (2004). *Sci. Technol. Adv. Mater.* **5**, 635.
15. H. Wang (2010). *Chin. J. Chem.* **28**, 1897.
16. Y. Z. Lan, W. D. Cheng, D. S. Wu, X. D. Li, H. Zhang, Y.-J. Gong, J. Shen, and F.-F. Li (2005). *J Mol. Struc.* **730**, 9.
17. A. Hirsch, (Thieme, 1994).
18. T. H. Fang, T. H. Wang, D. M. Lu, and W. C. Lien (2008). *Microelectron J.* **39**, 1600.
19. F. Trani, M. Causa, S. Lettieri, A. Setaro, D. Ninno, V. Barone, and P. Maddalena (2009). *Microelectron J.* **40**, 236.
20. W. H. Moon, M. S. Son, and H. J. Hwang (2007). *Appl. Surf. Sci.* **253**, 7078.
21. D. Farmanzadeh and S. Ghazanfary (2009). *Struct. Chem.* **20**, 709.
22. C. Attaccalite, L. Wirtz, A. Marini, and A. Rubio (2007). *Phys. Status Solidi B* **244**, 4288.
23. Q. Yuan and Y.-P. Zhao (2009). *Biomicrofluidics* **3**, 022411.
24. Q. Yuan and Y.-P. Zhao (2009). *J. Am. Chem. Soc.* **131**, 6374.
25. M. T. Baei, A. Soltani, A. V. Moradi, and M. Moghimi (2011). *Monatsh Chem.* **142**, 573.
26. M. T. Baei, A. Soltani, A. V. Moradi, and E. Tazikeh Lemeski (2011). *Comput. Theoret. Chem.* **970**, 30.
27. K. H. Khoo, M. S. C. Mazzoni, and S. G. Louie (2004). *Phys. Rev. B* **69**, 201401.
28. G. Y. Guo, S. Ishibashi, T. Tamura, and K. Terakura (2007). *Phys. Rev. B* **75**, 245403.
29. M. Machado and S. Azevedo (2011). *Eur. Phys. J. B* **81**, 121.
30. M. Schmidt, et al. (1993). *J. Comp. Chem.* **14**, 1347.
31. M. Mirzaei and M. Yousefi (2012). *Superlattic. Microstruct.* **52**, 612.
32. A. Ahmadi Peyghan, N. Hadipour, and Z. Bagheri (2013). *J. Phys. Chem. C* **117**, 2427.
33. A. Soltani, M. T. Baei, E. Tazikeh Lemeski, and A. A. Pahlevani (2014). *Superlattic. Microstruct.* **75**, 716.
34. S. F. Boys and F. Bernardi (1970). *Mol. Phys.* **19**, 553.
35. R. G. Parr, L. Szentpaly, and S. Liu (1999). *J. Am. Chem. Soc.* **121**, 1922.
36. F. Tournus and J. C. Charlier (2005). *Phys. Rev. B* **71**, 165421.
37. T. Koopmans (1993). *Physica* **1**, 104.
38. J.-X. Zhao, B. Gao, Q.-H. Cai, X.-G. Wang, and X.-Z. Wang (2011). *Theor. Chem. Acc.* **129**, 85.
39. Z. Li and C.-Y. Wang (2006). *Chem. Phys.* **330**, 417.
40. A. Soltani, M. T. Baei, M. Ramezani Taghartapeh, E. Tazikeh Lemeski, and S. Shojaee (2015). *Struct. Chem.* **26**, 685.
41. A. Soltani, M. T. Baei, M. Mirarab, M. Sheikhi, and E. Tazikeh Lemeski (2014). *J. Phys. Chem. Solids* **75**, 1099.
42. E. N. C. Paura, W. F. da Cunha, J. B. L. Martins, G. M. Silva, L. F. Roncaratti, R. Gargano (2014) RSC doi: 10.1039/C4RA00432A.
43. D. Farmanzadeh and S. Ghazanfary (2014). *Appl. Surf. Sci.* **320**, 391.